Probing the electrostatic potential of charged dislocations in *n*-GaN and *n*-ZnO epilayers by transmission electron holography

E. Müller* and D. Gerthsen
Laboratorium für Elektronenmikroskopie, Universität Karlsruhe (TH) 76128 Karlsruhe, Germany

P. Brückner and F. Scholz
Abteilung Optoelektronik, Universität Ulm, D-89069 Ulm, Germany

Th. Gruber
Abteilung Halbleiterphysik, Universität Ulm, D-89069 Ulm, Germany

A. Waag
Institut für Halbleitertechnik, Universität Braunschweig, D-38106 Braunschweig, Germany
(Received 14 February 2006; published 14 June 2006)

Epitaxial layers frequently contain a high density of threading dislocations, which may exceed values of 10^9 cm^{-2} for ZnO and GaN. To study the electrical activity of single dislocations off-axis electron holography in a transmission electron microscope was applied. The electrostatic potential in the vicinity of charged dislocations was determined from the reconstructed phase of the electron wave, which also provides access to the charge density at the dislocation. On the basis of the electrostatic potential for a screened line charge given by Read [Philos. Mag. **45**, 775 (1954)] a refined model is proposed in which a charge density with a finite spatial distribution at the dislocation core is assumed. Comparing the measured and theoretically expected potential, charge densities between 5×10^{19} cm^{-3} and 5×10^{20} cm^{-3} in cylinders with radii up to 5 nm around the dislocation lines were found. An important aspect of our work is the analysis of dislocations in cross-section transmission electron microscopy samples where the dislocation lines are oriented perpendicular to the electron beam. The advantages and drawbacks of the cross-section geometry are discussed. Electrostatic potentials due to piezoelectric charges in the dislocation strain field are considered and found to be insignificant with respect to dislocation charges.

DOI: 10.1103/PhysRevB.73.245316 PACS number(s): 61.82.Fk, 61.72.Ff, 73.43.Fj, 61.14.Nm

I. INTRODUCTION

Epitaxial GaN and ZnO layers are the basis of numerous (opto)electronic devices and sensor systems. In particular GaN-based heterostructures are already exploited commercially on a large scale for the fabrication of light-emitting devices and high-power electronic amplifiers. The large exciton binding energy of 60 meV of ZnO promises stimulated emission at room temperature which has triggered significant efforts to grow ZnO-based heterostructures by various epitaxial techniques in recent years.[1] However, despite considerable success in optimizing the epitaxial growth and structural quality, epitaxial layers still contain a high density of defects. Threading segments of misfit dislocations induced by the lattice-parameter mismatch between substrate and epilayer contribute significantly to the degradation of the optoelectronic properties and lead to a strong reduction of the charge carrier mobility.

The structural properties of threading dislocations—Burgers vectors and line directions—in GaN epilayers have been investigated in some detail by transmission electron microscopy (TEM), e.g., by Wu *et al.*[2] Edge, screw, and mixed dislocations were found with Burgers vectors of the type $1/3\langle 11\bar{2}0\rangle$, $\langle 0001\rangle$, and $1/3\langle 11\bar{2}3\rangle$ as expected for materials occurring in the wurtzite structure. The dislocation lines are oriented predominantly along the [0001]-growth direction. The fractions of different dislocation types depend on the parameters during epitaxial growth. Comparable morphologies were observed for threading dislocations in ZnO epilayers by Vigué *et al.*[3]

As reviewed already in 1991 by Alexander and Teichler[4] it has been known for many years that the electronic properties of dislocations in a semiconductor can be described by a (partially filled) band of electronic states in the energy gap. A simple model to explain the electrical activity of dislocations is illustrated by Fig. 1 assuming a partially filled band of electronic states which lies in the middle of the energy gap. The dislocation states will be only neutral if the occupation limit of the band E_{dis} coincides with the Fermi level E_f [Fig. 1(a)]. In *n*-type semiconductors, empty dislocation states are filled with electrons [Fig. 1(b)] until the occupation limit E_{dis} reaches E_f. The interaction of the excess charges along the dislocation generates an electrostatic potential V_{dis} with a maximum value V_B leading to a local bending of the band structure in the vicinity of the dislocation. For *p*-type semiconductors positive excess charges are accumulated at the dislocation core causing a bending of the band structure in the opposite direction [Fig. 1(c)].

The electrical activity of dislocations has been investigated almost exclusively by averaging techniques as, e.g., Hall mobility measurements. Look *et al.*[5] analyzed the Hall mobility of GaN samples containing dislocations with a density of 10^8 and 2×10^{10} cm^{-2}. Assuming one acceptor state per *c*-lattice parameter along the dislocation line they ob-

 ©2006 The American Physical Society

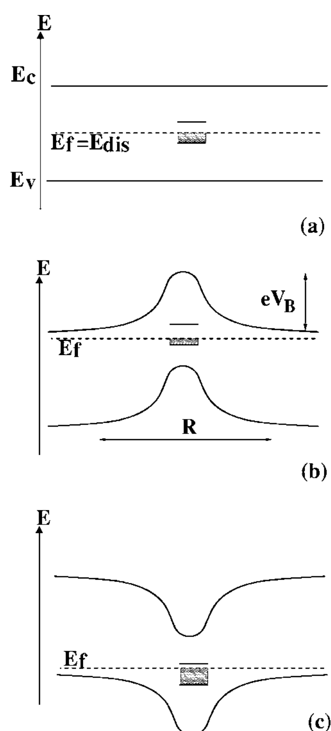

FIG. 1. Schematic model of the charging of dislocations in a crystal. The additional electronic states introduced by the dislocation bend locally the band structure of the crystal generating a potential barrier eV_B.

tained a good agreement between experimental and calculated electron mobilities. Only sparse information is available on the electrical properties of dislocations in ZnO. Osip'yan *et al.*[6] applied charge measurements during plastic deformation to analyze electrical charges associated with moving dislocations in bulk *n*-ZnO. They deduced a line charge of approximately 2 e/nm. However, the structure and electronic properties of glissile dislocations induced by plastic deformation may differ significantly from immobile threading dislocation in epilaxial layers—the latter being aligned predominantly along the [0001]-growth direction.

The electrical activity of individual dislocations has been studied traditionally by electron-beam induced currents (EBIC) (Ref. 7) or cathodoluminescence in a scanning electron microscope. Applying cathodoluminescence, an enhanced recombination activity was revealed for dislocations in ZnO by Vasnyov *et al.*[8] which is a strong indication for electrically active dislocations.

The electrical potential associated with single dislocations became accessible only recently when Cherns and Jiao[9] applied electron holography in a transmission electron microscope to detect the electrostatic potential V_{dis} in the vicinity of single dislocations in GaN which they associated with a negatively charged dislocation core in *n*-GaN. The same technique was used to compare the charge at dislocations depending on the doping of the material.[10] It was shown that edge dislocations are negatively charged in *n*-doped GaN, whereas those in *p*-doped GaN are positively charged. Electron holography investigations of different dislocations types in *n*-conducting GaN were perfomed by Cai and Ponce.[11] Using a cross-section TEM sample they obtained negative charge densities of 1, 0.3, und 0.6 e/c for screw, edge, and mixed dislocations with extended charged core radii.

The reconstruction of the phase shift of the electron wave ϕ, which is measured with respect to the phase of a reference wave, allows to deduce V_{dis} on the basis of Eq. (1) (see, e.g., Reimer, Ref. 12)

$$\phi = C_E \int_0^t (V_0 + V_{\mathrm{dis}}(\vec{r}))dz, \tag{1}$$

where V_0 is the mean inner Coulomb potential of the material and C_E is a constant depending on the electron energy. The integration has to be performed along the electron-beam direction over the sample thickness t. It has to be emphasized that Eq. (1) is only valid if kinematical diffraction conditions are applied because dynamical electron diffraction imposes additional phase shifts. As further outlined in Sec. II, the electrostatic potential V_{dis} depends mainly on the charge density at the dislocation core and the screening charge density in the vicinity of the dislocation. This additional potential affects only the phase of the analyzing electron wave and is not directly accessible by classical imaging methods.

In the present work we have analyzed the electrical activity of individual dislocations in *n*-ZnO and *n*-GaN epilayers using TEM combined with off-axis electron holography. The study was motivated partially by the difficulty to obtain *p*-conducting ZnO because charged dislocations do not only reduce the charge carrier mobility but can also provide a high density of electronic states if the dislocation density is high as in the case of epitaxial *n*-ZnO layers. This contribution needs to be taken into account in the overall charge balance of the material. On the basis of the reconstructed phase of the electron wave the electrostatic potential V_{dis} and the charge density was determined considering in particular the possible formation of piezoelectric charge densities. For this purpose we refined the model for V_{dis} suggested originally by Read.[13] A further motivation was the assessment and possible improvement of the accuracy for the measurement of the electrostatic potential introduced by charged dislocations.

II. ELECTROSTATIC POTENTIAL OF A CHARGED DISLOCATION

A model for the electrostatic potential of a charged dislocation was already proposed by Read[13] in 1954. He assumed an uniformly distributed line charge along the dislocation line with a density q which is given in the following in units of nm^{-1}. To obtain overall neutrality of the sample this charge is screened by a cylinder with a space charge density of opposite sign. Solving the Poisson equation under adequate boundary conditions yields the potential V_R inside the space charge cylinder which is given by Eq. (2),

$$V_R(r) = \frac{-qe}{4\pi\varepsilon\varepsilon_0}\left[\ln\left(\frac{r^2}{R^2}\right) - \left(\frac{r^2}{R^2}\right) + 1\right], \tag{2}$$

where $r=\sqrt{x^2+z^2}$ is the distance from the dislocation core. The radius of the space charge cylinder $R=\sqrt{q/\pi N_s}$ is determined by q and the density of the compensating charges of

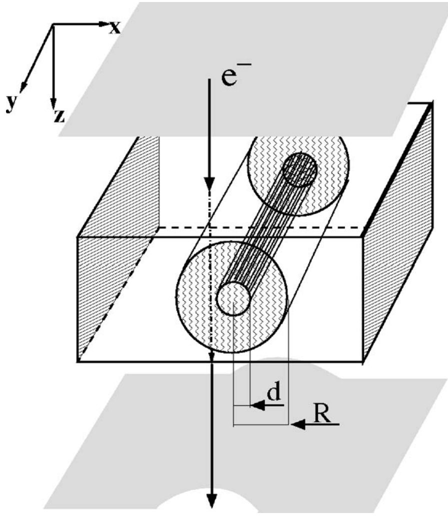

FIG. 2. Schematic drawing illustrating the charge configuration for the refined Read potential and the interaction of an incident plane electron wave with a thin TEM sample containing a charged dislocation.

opposite sign N_s, which are available for screening.

We have refined Read's potential by replacing the line charge density q by a space charge density ρ in a small inner cylinder with the radius d around the dislocation core which is schematically shown in Fig. 2. The charges at and in the close vicinity of the dislocation core are screened by a space-charge region of opposite sign. The electrostatic potential of this configuration is given by Eqs. (3) for different distances r from the dislocation core,

$$V_{\mathrm{dis}}(r) = \begin{cases} \frac{-\rho d^2 e}{4\varepsilon\varepsilon_0}\left[\ln\left(\frac{d^2}{R^2}\right) - \left(\frac{r^2}{R^2}\right) + \left(\frac{r^2}{d^2}\right)\right] & \text{for } r < d \\ \frac{-\rho d^2 e}{4\varepsilon\varepsilon_0}\left[\ln\left(\frac{r^2}{R^2}\right) - \left(\frac{r^2}{R^2}\right) + 1\right] & \text{for } d \leqslant r \leqslant R \\ 0 & \text{for } r > R. \end{cases} \quad (3)$$

The radius of the space charge cylinder is determined by ρ and the density of the compensating charges N_s,

$$R = d\sqrt{\rho/N_s}. \quad (4)$$

For dislocation states with acceptor character in n-type semiconductors, N_s is given by the density of uncompensated donors in the vicinity of the dislocations. Outside of the screening radius R, the potential is set to zero.

In contrast to the Read potential which is characterized by a singularity at $r=0$ the modified model of the charged dislocation provides the possibility to calculate the deformation of the band structure at the dislocation core. Using the first of Eqs. (3) which represents the potential V_{dis} close to the dislocation core the potential barrier $V_B = V_{\mathrm{dis}}(r=0)$ is given by

$$eV_B = \frac{-\rho d^2 e^2}{4\varepsilon\varepsilon_0}\ln\left(\frac{d}{R}\right)^2. \quad (5)$$

In the limit of a small dislocation core radius compared to the screening radius R ($d \ll R$) the charge density $\rho\pi d^2$ becomes a line charge with density q and the Read potential Eq. (2) is obtained. If V_B and the Fermi energy E_f is known, the location of the electronic states associated with the dislocations E_{dis} can be readily determined according to Eq. (6),

$$E_{\mathrm{dis}} = E_f - eV_B. \quad (6)$$

The phase shift that will be detected by electron holography according to Eq. (1) depends on the integrated potential, i.e., the orientation of the dislocation relative to the path of the analyzing electron wave. Orienting the dislocation parallel to the electron beam along the z axis (edge-on configuration), $V_{\mathrm{dis}}(r=\sqrt{x^2+y^2})$ is constant along the electron path and leads to the phase shift,

$$\phi(x,y) = C_E(V_0 + V_{\mathrm{dis}}(x,y))t. \quad (7)$$

An orientation of the dislocation perpendicular to the electron beam requires the integration of the potential given by Eqs. (3) which varies along the integration path. Despite this difficulty we will show, that the cross-section perspective may even provide some advantages although the phase shift is not maximized.

III. EXPERIMENTAL TECHNIQUES

All investigated samples were grown by low pressure metal organic vapor phase epitaxy (MOVPE) on $Al_2O_3(0001)$ substrates. The ZnO layer was deposited on an $Al_2O_3(0001)$ substrate with 40 nm GaN as a buffer layer between the substrate and the ZnO. The substrate temperature was 380 °C during the ZnO deposition and isopropanol and diethylzinc were used as precursors with a VI/II-flux rate ratio of 36.

The GaN layer was deposited at 1125 °C on a low-temperature AlN nucleation layer using the standard precursors trimethylgallium, trimethylaluminum, and NH_3. Silane was used as an n-type dopant source. By van der Pauw Hall effect measurements, a carrier concentration of 2×10^{19} cm^{-3} and a mobility of 116 cm^2/V s was determined.

The TEM investigations were carried out in a 200 keV Philips CM 200 FEG/ST microscope which is equipped with a field emission gun. The dislocation Burgers vectors $\vec{b}$ were analyzed on the basis of the $\vec{b}\vec{g}=0$ extinction criterion using different imaging vectors $\vec{g}$. The weak-beam technique was applied to improve the resolution compared to conventional bright-field and dark-field images (see, e.g., Ref. 14). Cross-section samples along the $\langle 1\bar{1}00\rangle$ and $\langle 11\bar{2}0\rangle$ zone axes were prepared applying the technique described by Strecker *et al.*[15] To minimize radiation damage the acceleration voltage during Ar^+-ion milling was stepwise reduced from 3.5 keV to 2.0 keV in the final stage of the ion milling.

For off-axis electron holography, the microscope is equipped with a Möllenstedt-Düker biprism, which is installed in the selected-area aperture holder. The electrostatic potential of the biprism was set to approximately 150 V leading to an interference fringe distance of 0.2 nm which was sampled by 5.6 pixels/fringe using a 2048×2048 pixel

CCD camera. Holograms were obtained by orienting a straight dislocation line parallel to the biprism whereas the reference wave is transmitted through the undisturbed crystal on the other side of the biprism. The known lattice fringe distance of high-resolution TEM images was used to calibrate accurately the microscope magnification. More details about the experimental procedures and reconstruction of the amplitude and phase of the electron wave from the hologram are outlined by Lehmann and Lichte.[16]

To suppress phase shifts due to dynamical electron scattering, kinematical diffraction conditions must be applied. This can be achieved by tilting the sample with respect to the electron beam in such a way that strongly excited reflections are not observed in the diffraction pattern. However, it must be taken into account that the orientation of the lattice is tilted in the vicinity of dislocations, which requires special attention as will be further discussed in Sec. V C.

In addition, phase changes in the vicinity of the dislocation line can be induced by thickness variations of the TEM sample. As the dislocations are completely embedded in the TEM samples, the formation of pits at the intersection between the dislocation and the surface due to preferential Ar^+-ion thinning during TEM sample preparation is avoided.

IV. EXPERIMENTAL RESULTS

Figure 3 shows bright-field overview images of the same region of the *n*-GaN layer on a $(0001)Al_2O_3$ substrate in cross-section perspective. The dislocations are aligned predominantly along the $[0001]$ direction. Applying different imaging vectors allows the distinction of the different dislocation types. Screw and mixed dislocations are visible in Fig. 3(a) which was taken with an imaging vector $\vec{g}=[0002]$. Edge and mixed dislocations are in contrast in Fig. 3(b) for $\vec{g}=[11\bar{2}0]$.

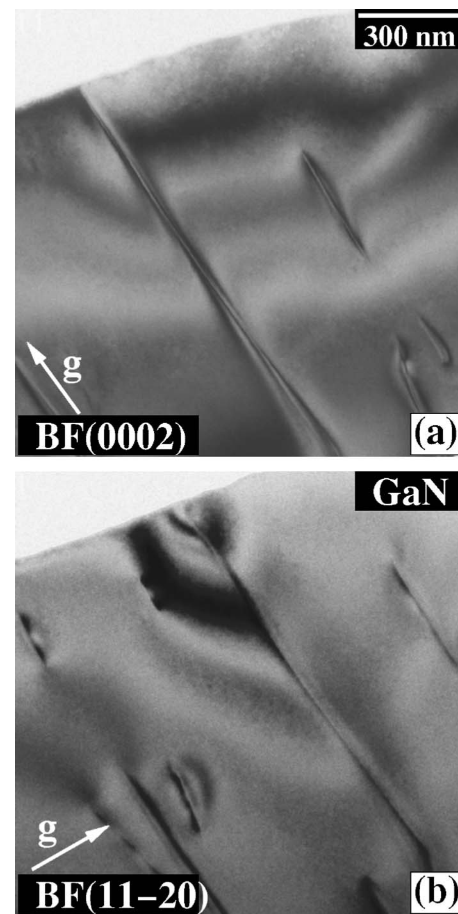

FIG. 3. Bright-field TEM images of a GaN cross-section sample taken with imaging vectors (a) $\vec{g}=[0002]$ and (b) $\vec{g}=[11\bar{2}0]$.

The analysis of cross-section samples leads to a perpendicular alignment of the dislocations relative to the electron-beam direction. Figure 2 shows schematically the interaction of an incident plane electron wave propagating along the z direction with the electrostatic potential in the vicinity of a dislocation. After the transmission of the electron wave through the thin TEM sample the analyzing electron wave is modified in amplitude and phase. Assuming a negatively charged dislocation line and positive charges in the screening cylinder, the electron wave is locally retarded compared to the surrounding neutral bulk region. This induces a local distortion of the plane wave, which can be detected by electron holography as a phase shift if the potential is strong enough.

Figure 4 shows results obtained for the *n*-GaN epilayer. The grey-scale coded phase of a sample region containing a mixed dislocation with a Burgers vector of the type $1/3\langle 11\bar{2}3\rangle$ is displayed in Fig. 4(a). The orientation of the dislocation is indicated by the dashed line. To increase the signal to noise ratio and to ensure that the reference wave is transmitted through an undisturbed region of the sample with constant thickness, we usually take two holograms of the dislocation, shifting the sample slightly between the two images. Subsequently, line scans perpendicular to the dislocation line are performed from the phase images, averaging typically several nm along the dislocation line (y coordinate). The line scans from the two holograms are then correlated and averaged. A distinct phase shift can be recognized in the phase profile perpendicular to the dislocation line shown in Fig. 4(b).

To deduce the charge density at the dislocation core from the measured phase we use Eqs. (1), (3), and (4) to calculate the potential V_{dis} from the phase profile given in Fig. 4(b). The interaction constant C_E in Eq. (1) is $7.29\times 10^6\ \text{rad V}^{-1}\ \text{m}^{-1}$ for our microscope (Ref. 17). The electrical permittivity ε was taken to be 9.5 for GaN (Ref. 18) and 7.8 for ZnO (Ref. 19). If the hologram interference pattern, which limits the field of view to approximately 50 nm, is wide enough, the radius R of the screening cylinder can be measured directly from the phase shift perpendicular to the dislocation line as indicated in Fig. 4(b). We then treat the line charge density ρ and d as fit parameters and calculate N_s from Eq. (4). If the free charge carrier concentration n_C is known from electrical measurements and $n_c\approx N_s$ is assumed, only one of the two parameters ρ or d is left to be fitted. A free electron density $n_c=2\times 10^{19}$ (elementary charges) cm^{-3} was determined by van der Pauw Hall measurements for the *n*-GaN sample which is taken as a first estimate for N_s. However, we obtain $d=15$ nm for the inner

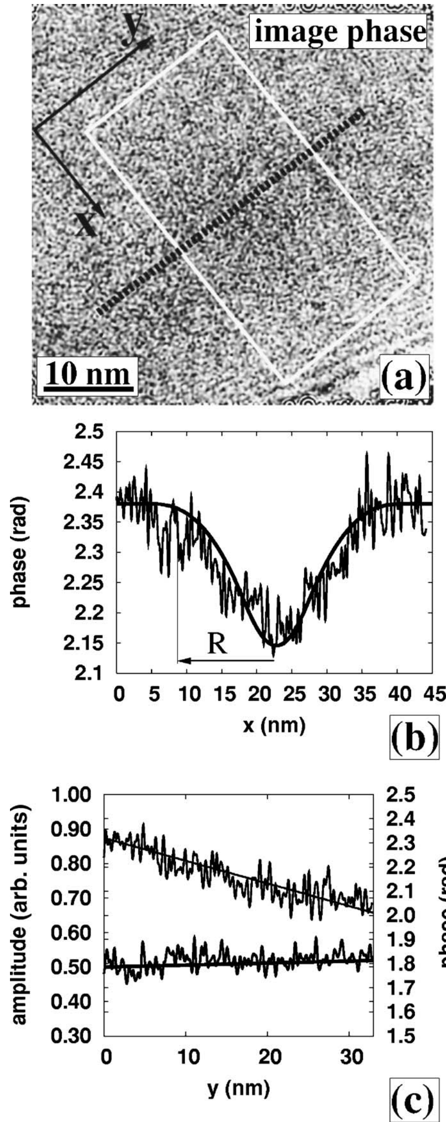

FIG. 4. Analysis of a dislocation with $\vec{b}=1/3\langle 11\bar{2}3\rangle$ in n-GaN: (a) gray-scale coded reconstructed phase of the electron wave with the dislocation line direction indicated by the dashed line, (b) phase plotted as a function of the x direction as defined in (a) perpendicular to the dislocation line. To reduce the noise, the phase was averaged along the y direction within the frame marked in (a). (c) Phase (upper curve) and amplitude profiles parallel to the dislocation line. The variation of the phase is proportional to the thickness variation while the amplitude is opposite to it.

charge cylinder with this N_s value which appears unrealistically large. Alternatively, the fit was performed without an assumption for N_s. With the measured radius of the screening cylinder $R=18$ nm, a charge density $\rho=7.2\times 10^{19}$ cm^{-3} with a radius $d=5$ nm is derived for the charge cylinder around the dislocation core. These values correspond to a density of compensating charges $N_s=6.0\times 10^{18}$ cm^{-3} and a potential barrier $V_B=2.2$ V. The line in Fig. 4(b) represents the best fit on the basis of Eqs. (1), (3), and (4). The discrepancy of N_s with respect to the free electron concentration could be related to a local variation of the concentrations of electrically active point defects in the dislocation strain field with respect to the undisturbed bulk material.

The sign of the phase shift, which is determined by the sign of the dislocation charges, is not obvious because the digital reconstruction of the amplitude and phase of the image wave provides two side bands in the Fourier transformation of the holograms. The phase is stored with opposite sign in these side bands (Ref. 16). To determine the correct sign of the phase profile in our experimental situation where a vacuum reference region is not available in the same hologram with the dislocation, the amplitude of the image wave has to be evaluated as well. If a thickness gradient is present in the analyzed region, the variation of the amplitude and the phase has to reveal an opposite sign, if the reconstruction is performed with the proper sideband. In the case of the wrong sideband the gradient of the amplitude and the phase would be the same.[20] To determine the sign of the dislocation charge, a line scan was performed parallel to the dislocation line where the contribution of the charged cylinder is expected to be constant. Figure 4(c) shows the variation of the amplitude and the phase parallel to the dislocation line. Despite the noisy signal, the sign of the gradients for the amplitude and the phase are clearly opposite which shows that the proper sideband was used for the reconstruction of the image wave. The negative phase shift with respect to the bulk reference wave demonstrates that negative charges are localized in the vicinity of the dislocation core.

The energy levels associated with the dislocation can be calculated according to Eq. (6) because the free electron concentration n_c is known. The density of states of the conduction band for GaN is given by[21]

$$N_C = 2.5\times 10^{19}\left(\frac{m_e^*}{m_0}\right)^{3/2}\left(\frac{T[\mathrm{K}]}{300}\right)^{3/2}. \tag{8}$$

With the relative effective electron mass in the conduction band $m_e^*/m_0=0.22$ the density of conduction band states at room temperature is $N_C=2.6\times 10^{18}$ cm^{-3}. Since N_C is lower than n_c degenerate conditions apply and the Fermi energy is located above the conduction band edge. The position of the Fermi energy can be calculated approximately according to Dixon and Joycs[22] by Eq. (9),

$$\frac{E_F-E_c}{k_BT}\cong \ln\frac{n_C}{N_C}+\frac{1}{\sqrt{8}}\frac{n_C}{N_C}-\left(\frac{3}{16}-\frac{\sqrt{3}}{9}\right)\frac{n_C^2}{N_C^2}+\cdots, \tag{9}$$

where E_c denotes the conduction band edge. With $E_f-E_c=5.12\ k_BT=0.13$ eV and $eV_B=2.19$ eV we obtain $E_c-E_{\mathrm{dis}}=2.32$ eV, i.e., acceptor states associated with the dislocation are localized well in the lower half of the energy gap of GaN.

Analogous experiments were carried out for dislocations in the n-ZnO expilayer. The gray-scale coded phase of a sample region containing an edge dislocation with a Burgers vector of the type $\frac{1}{2}\langle 11\bar{2}0\rangle$ is displayed in Fig. 5(a). The orientation of the dislocation is indicated by the dashed line. The phase profile perperdicular to the dislocation line is displayed in Fig. 5(b) from which we determine the radius of the screening cylinder $R=25$ nm. The line in Fig. 5(b) represents the best fit for a space charge density of approximately 7.0×10^{19} cm^{-3} for a charged dislocation cylinder

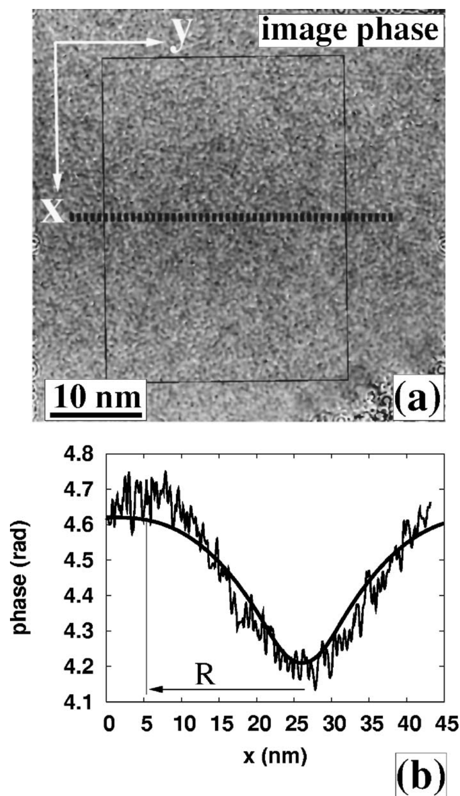

FIG. 5. Analysis of an edge dislocation in n-ZnO: (a) gray-scale coded reconstructed phase of the electron wave with the dislocation line direction indicated by the dashed line, (b) phase plotted as a function of the x direction as defined in (a) perpendicular to the dislocation line. To reduce the noise the phase was averaged along the y direction within the frame marked in (a).

with $d=5$ nm. The sign of the charges is negative. The charges yield a potential barrier $V_B=3.2$ V for a screening charge density of $N_s=2.9\times10^{18}$ cm^{-3}.

The charge densities and radii d vary for different analyzed dislocations between $\rho=5\times10^{19}$ cm^{-3} and $\rho=5\times10^{20}$ cm^{-3} in an extreme case. The latter charge density is confined within a charge cylinder with $d=1.5$ nm. These different charge densities should not be associated with strongly different dislocation charge states because the effective line charge is determined by the prefactor $\rho\pi d^2$ in Eq. (3) which was found to be 5.7 nm^{-1} for n-GaN and 5.5 nm^{-1} for n-ZnO for the holograms with the best quality.

V. DISCUSSION

A. Charge at dislocations in *n*-ZnO and *n*-GaN

A strong electrostatic potential was detected in the vicinity of dislocations in n-ZnO and n-GaN indicating that charges are accumulated at or close to the dislocation core. The measured phase profiles can be fitted reasonably well using the theoretically calculated potential of a screened charge cylinder around a dislocation. Charge densities between 5×10^{19} and 5×10^{20} cm^{-3} within charge cylinders with radii up to 5 nm were repeatedly derived for dislocations with edge-components in n-GaN and n-ZnO. We could not obtain data for pure screw dislocations.

To compare formally our values for the dislocation charge densities with the data of previous work (Refs. 9–11) we can convert the volume density at the dislocation core within radius d to line charge densities by the relation $q=\rho\pi d^2$. We obtain values up to 5 nm^{-1} which are slightly higher than those of Cherns *et al.*[9,10] These differences can be understood by the different models which were used for the evaluation of the experimental data and also by the error margins of the procedure. Cherns *et al.*[9,10] assumed a line charge density without permitting an extended dislocation core in contrast to the finite dislocation core in our evaluation. Cai and Ponce[11] obtained lower values for the charge density although they permitted an extended dislocation core. However, in their evaluation of the line charge density a constant potential and charge density was assumed through the whole sample thickness which is not valid for the analysis of dislocations in the cross-section geometry.

The physical origin of this charge is not obvious. Elsner and Jones[23] have calculated that threading screw and threading edge dislocations in wurtzite GaN are electrically inactive. Thus it it more likely that possible sources of these charges are point defects, which are accumulated in the strain field around the dislocation core. The relatively large radii d up to 5 nm for the charged dislocation cylinders, could indeed be an indicator for the dominant role of point defects. The large variations of the charge densities ρ could reflect local variations of point defect concentrations in the vicinity of the dislocations. For GaN, Ga vacancies V_{Ga} and $V_{\mathrm{Ga}}/\mathrm{O}$ complexes were suggested as possible candidates.[24,25] Acceptor character was attributed to both types of defects consistent with a negative dislocation charge which we observe.

Since piezoelectricity is strong in GaN and ZnO, another possible source of electrical activity are polarization charges in the dislocation strain field. Shi *et al.*[26] already analyzed the expected polarization of screw, edge, and mixed dislocations in GaN. They showed that piezoelectrically induced charges do not occur for dislocations with [0001]-line directions. However, electrical charges are expected at the intersection of edge- and mixed-type dislocations with the surface or at interfaces due to the difference of the electrical permittivities. We will show in the next section that these charges are either too small to be detected by electron holography or can be identified by the typical shape of the resulting potential.

Another contribution to the error $\Delta\rho$ is related to the value of the static electrical permittivity for which values between 7 and 8.6 are published in the case of ZnO. Additionally, if the thickness of the sample is smaller than the diameter of the screening cylinder, the electrostatic field leaks into the vacuum region with a dielectric constant of 1, much lower than in the bulk material, which would lead to higher values of the charge density. This would be demanded for the knowledge of the sample thickness and the position of the dislocation in the material with respect to the radius of the screening cylinder and a modification of the model by considering two different values of the permittivity within the appropriate volume fraction. In general lower charges would be the result. The model will fail at extremely high dislocation densities if the space charge regions overlap. However,

such a case could be detected by the measurement of the free charge carrier density which would be extremely low.

B. Piezoelectric charge density associated with dislocations

It must be expected that piezoelectric charges are generated in the strain field of dislocations in ZnO and GaN which are both materials with large piezoelectric constants e_{ij}. A theoretical study of the piezoelectric effect associated with the c axis oriented dislocations in wurtzite GaN by Shi *et al.*[26] showed that the polarization field of dislocations with a screw component is divergence free and does not generate an electric field. Edge dislocations produce polarization fields with nonzero divergence at interfaces and surfaces. According to Ref. 26 the surface charge density for a c axis oriented edge dislocation intersecting the crystal surface is given by

$$q_s = \frac{b \cdot e_{31}}{2\pi} \frac{1-2\nu}{\nu-1} \frac{1}{r} \sin\varphi, \tag{10}$$

where b is the length of the Burgers vector of the dislocation, e_{31} is the relevant component of the piezoelectric tensor, and ν is the Poisson ratio given by $\nu = c_{12}/(c_{12}+c_{11})$. The calculation is performed in a cylindrical coordinate system with coordinates (r, φ, z). At a distance $r=10$ nm from the dislocation core the surface charge density of an edge dislocation reaches about $10^{12}\ e/\text{cm}^2$ for GaN (Ref. 26). An analogous calculation for an edge dislocation in n-ZnO yields $q_s = 1.1\times 10^{12}\ e/\text{cm}^2$ for $e_{31} = -0.62\ \text{C/m}^2$, $\nu = 0.318$ (according to Ref. 1), and $b = 0.325$ nm.

For the investigation performed in this work, the dislocations are oriented roughly parallel to the sample surface. If the dislocation lies close to the surface, screw dislocations are expected to generate surface charges as well. The piezoelectric polarization for a screw dislocation in c-axis orientation can be written as[26]

$$P_s = \frac{b \cdot e_{15}}{2\pi} \frac{1}{r} \hat{\varphi}. \tag{11}$$

The surface charge density corresponds to the component of the polarization perpendicular to the surface. Assuming that the normal component of the surface is $(0,1,0)^T$ the polarization in this direction is

$$P_s = \frac{b \cdot e_{15}}{2\pi} \frac{x}{x^2+y^2}. \tag{12}$$

Introducing the values $e_{15} = -0.37\ \text{C/m}^2$ from Ref. 1 and the Burgers vector $b = 0.520$ nm for ZnO a surface charge density of approximately $0.9\times 10^{12}\ e/\text{cm}^2$ is found at the distance $r=10$ nm from the dislocation core.

To estimate the contribution of surface charges to the phase shift of the analyzing electrons, the potential of the charges has to be integrated along the electron path. This task can no longer be solved analytically but requires numerical integration. The calculated potential perpendicular to the dislocation line is depicted in Fig. 6. We have assumed here that the screw dislocation line is oriented parallel to the surface with a small distance of 10 nm between the dislocation and the surface. The phase shift of the electrons passing through this surface is also contained in Fig. 6. It shows that the maximum phase shift is only marginally below the phase detection limit of 0.08 rad. This indicates that the piezoelectrical charges on the surface in the vicinity of a screw dislocation can induce additional phase shifts. However, the effect is small and can be distinguished from the phase shift from charged dislocations due to the characteristic sine-shaped phase distribution. Surface charges are not induced by edge dislocations parallel to a surface because the polarization component perpendicular to the surface vanishes.

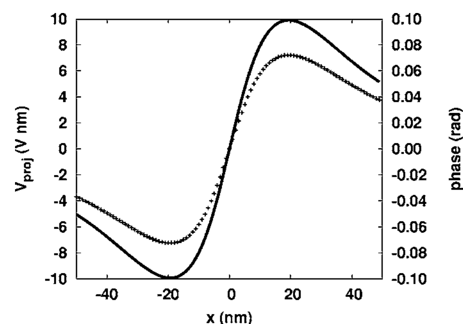

FIG. 6. Phase shift (dashed line) and projected potential (continuous line) due to piezoelectric charges on a surface parallel to a screw dislocation. The dislocation core is situated at a distance of 10 nm from the surface.

C. Methodical considerations

In contrast to previous holographic observations of dislocations (Ref. 9) where the dislocations were oriented parallel to the electron beam we use cross-section TEM samples where the dislocations are aligned perpendicular to the electron beam. This was partially motivated by the fact that it was not possible to prepare good quality planview samples for ZnO heterostructures. An obvious drawback of the cross-section geometry is the relatively high charge density, which is required to exceed the phase detection limit. However, there are also advantages connected with the cross-section geometry with respect to obtaining quantitative data for the line charge density.

In cross-section geometry, a precise knowledge of the mean inner potential of the material is not required to determine V_{dis}. In addition, the sample thickness does not need to be known accurately because the integration in Eq. (1) has to be carried out only over the diameter of the space charge cylinder $2R$ which can be directly measured as shown in Sec. IV. Inside of the space charge region the charged dislocation generates an additional phase shift which is superimposed on the phase shift due to the mean inner potential. Provided that the local sample thickness does not change significantly, the latter only introduces a constant offset to the image phase.

In cross-section geometry dislocations are typically embedded in the material which prevents the formation of pits which are generated frequently by ion milling during TEM sample preparation at the intersection between the dislocation and the surface. If pits are present, the resulting phase shift in the vicinity of the dislocation core would be decreased with respect to the surrounding bulk material.

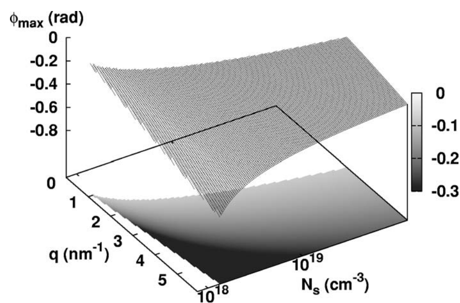

FIG. 7. Maximum phase shift due to a charged dislocation oriented perpendicular to the electron beam represented as a surface depending on the screening charge density N_s and the line charge density q. Due to the limited field of view and the phase detection limit of 0.08 rad the surface is truncated. The projection of the truncated phase surface provides the detectable range of line charges q in dependence of the available density of screening charges N_s. The gray-scale coding of the projected surface represents the maximum phase shift.

Moreover, phase shifts induced by dynamical electron diffraction are easier to control for dislocations in cross-section geometry. Kinematical diffraction conditions are typically adjusted by tilting the sample in such a way that the intensity of (bulk) Bragg reflections is minimized. However, the lattice is tilted in the vicinity of dislocation core by the dislocation strain field, and kinematical diffraction conditions for the surrounding bulk material may not necessarily be sufficient to suppress local dynamical phase shifts around the dislocation. In cross-section geometry, the analyzing electron wave encounters the tilted crystal region only in the vicinity of the dislocation along a short path. It can be also shown, that dynamical phase shifts are negligible even under $(g,4g)$ weak-beam conditions for $\vec{g}=\langle 11\bar{2}0\rangle$ and $\langle 1\bar{1}00\rangle$ by solving numerically the Howie-Whelan equations (see, e.g., Ref. 14) for edge and screw dislocations. Working under $(g,4g)$ weak-beam conditions simplifies hologram recording due to the improved visibility of the dislocation compared to the fully kinematical mode. In contrast, dynamical phase shifts in the vicinity of the dislocation core may be accumulated in planview geometry over the whole specimen thickness although kinematical diffraction conditions apply for the surrounding bulk material.

The main disadvantage associated with dislocations aligned perpendicular to the electron beam, is the small optical path difference which prevents the detection of weakly charged dislocations due to the phase detection limit of 0.08 rad. As our electron microscope is not equipped with a Lorentz lens, another limitation is imposed by the width of the analyzable region of the hologram which is restricted to 50–60 nm. Taking these two restrictions into account, the detectable charge densities in the cross-section mode are plotted in Fig. 7. The surface represents the maximum phase shift $\phi_{\max}$ induced by a charged dislocation depending on the line charge density q and the screening charge density N_s.[27] This phase shift is truncated at $\phi=0.08$ rad which represents the phase detection limit. The surface is also truncated laterally by the condition that the detectable screening length R is restricted to approximately 25 nm. For a given value q the latter restriction implies a particular densitiy of the screening charges N_s because R, q, and N_s are linked by the equation $R=\sqrt{q/\pi N_s}$. The projection of the truncated phase surface on the base plane of Fig. 7 shows the range of detectable line charge densities q which depend on the screening charge density N_s. The gray-scale coding of the projected surface gives that maximum phase shift. The minimum detectable line charge density lies at about 1 e/nm.

A general aspect that needs to be considered for measurements of electrostatic potentials by transmission electron holography was recently put forward by Houben *et al.*[28] It was pointed out that excess carrier generation by the electron beam can alter the electrostatic potential for equilibrium charge carrier concentrations below 10^{17} cm^{-3} for semiconductors with an indirect energy gap. However, the samples investigated in the present work are direct-gap semiconductors with a high free electron concentration and with a recombination time several orders of magnitude shorter than for silicon.[29] Thus we can exclude a detectable modification of the electrostatic potential. This was verified experimentally by taking several holograms of the same dislocation with different illumination intensities which did not change the observed phase shift.

VI. SUMMARY

Electron holography in a transmission electron microscope allows the quantitative measurement of electrostatic potentials in materials on the nanoscale. This capability was exploited to study the electrical activity of single threading dislocations in epitaxial n-ZnO and n-GaN layers. Cross-section samples were used in our study where the dislocations are oriented perpendicular to the electron beam. Despite the loss in sensitivity with respect to the detectable charge density compared to planview samples, quantitative results can be obtained with reasonable accuracy because we do not rely on accurate values of the local TEM sample thickness and the mean inner Coulomb potential of the material.

A refined Read model for charged dislocations was developed to describe the measured phase distribution perpendicular to the dislocation line. Assuming a volume charge density within a small charge cylinder around the dislocation core prevents the divergence of the electrostatic potential directly at the dislocation line. For epitaxial n-ZnO and n-GaN layers negative charge densities between 5×10^{19} and 5×10^{20} cm^{-3} within charge cylinders with radii up to 5 nm around the dislocation core were found. This corresponds to effective line charge densities $\rho\pi d^2$ up to 5 nm^{-1} for n-GaN and n-ZnO. The spatial extension of the charge around the dislocation core is a strong indicator that point defects in the vicinity of the dislocation core rather than intrinsic core states are responsible for the electrical acitivity of the dislocations. The electronic states associated with the dislocations are located in the lower half of the energy gap. Since we know the Fermi energy in the case of n-GaN an energy level

2.3 eV below the conduction band edge could be associated with the acceptor states of the analyzed dislocation. Piezoelectric charges due to the dislocation strain field were found to be insignificant for dislocations in cross-section TEM samples.

The high dislocation line charge in *n*-ZnO and *n*-GaN indicates that dislocations can provide electronic states with a high concentration. For a dislocation density of 10^9 cm^{-2} additional states with a density in the order of 5×10^{16} cm^{-3} are generated which need to be considered in the overall charge balance of the material.

ACKNOWLEDGMENTS

The work of E. Müller and D. Gerthsen is financially supported by the Landesstiftung Baden-Württemberg GmbH.

*Author to whom correspondence should be addressed. Electronic address: mueller@lem.uni-karlsruhe.de; Tel: +49 721 608 4889; Fax: +49 721 608 3721.

[1] Ü. Özgur, Ya. I. Alivov, C. Liu, A. Teke, M. A. Reshchikov, S. Dogan, V. Avrutin, S.-J. Cho, and H. Morkoc, J. Appl. Phys. **98**, 041301 (2005).

[2] X. H. Wu, L. W. Brown, D. Kapolnek, S. Keller, B. Keller, S. P. Den-Baars, and J. S. Speck, J. Appl. Phys. **80**, 3228 (1996).

[3] F. Vigué, P. Vennéguès, S. Vézian, M. Laügt, and J.-P. Faurie, Appl. Phys. Lett. **79**, 194 (2001).

[4] H. Alexander and H. Teichler, *Materials Science and Technology* (North-Holland, Amsterdam, 1991), Vol. 4, Chap. 6, p. 249.

[5] D. C. Look and J. R. Sizelove, Phys. Rev. Lett. **82**, 1237 (1999).

[6] Yu. A. Osip'yan, V. F. Petrenko, A. V. Zaretski, and R. W. Whitworth, Adv. Phys. **35**, 115 (1986).

[7] V. Kveder, M. Kittler, and W. Schröter, Phys. Rev. B **63**, 115208 (2001).

[8] S. Vasnyov, J. Schreiber, and L. Hoering, J. Phys.: Condens. Matter **16**, 269 (2004).

[9] D. Cherns and C. G. Jiao, Phys. Rev. Lett. **87**, 205504 (2001).

[10] D. Cherns, C. G. Jiao, H. Mokhtari, J. Cai, and F. A. Ponce, Phys. Status Solidi B **234**, 924 (2002).

[11] J. Cai and F. A. Ponce, Phys. Status Solidi A **192**, 407 (2002).

[12] L. Reimer, *Transmission Electron Microscopy* (Springer Verlag, Berlin, 1984), p. 21.

[13] W. T. Read, Philos. Mag. **45**, 775 (1954).

[14] D. B. Williams and C. B. Carter, *Transmission Electron Microscopy* (Plenum, New York, 1996).

[15] A. Strecker, U. Salzgeber, and J. Mayer, Prakt. Metallogr. **30**, 482 (1993).

[16] M. Lehmann and H. Lichte, Microsc. Microanal. **8**, 447 (2002).

[17] P. Kruse, A. Rosenauer, and D. Gerthsen, Ultramicroscopy **96**, 11 (2003).

[18] A. S. Barker, Jr. and M. Ilegems, Phys. Rev. B **7**, 743 (1973).

[19] Landolt-Börnstein, *Numerical Data and Functional Relationships in Science and Technology* (Springer-Verlag, Berlin, 1987), Vol. 22, p. 165.

[20] M. R. McCartney and M. Gajdardziska-Josifovska, Ultramicroscopy **53**, 283 (1994).

[21] H. Morcoc, *Nitride Semiconductors and Devices* (Springer-Verlag, Berlin, 1999), p. 220.

[22] W. B. Joyce and R. W. Dixon, Appl. Phys. Lett. **31**, 354 (1977).

[23] J. Elsner, R. Jones, P. K. Sitch, V. D. Porezag, M. Elstner, T. Frauenheim, M. I. Heggie, S. Öberg, and P. R. Briddon, Phys. Rev. Lett. **79**, 3672 (1997).

[24] J. Neugebauer and C. Van de Walle, Appl. Phys. Lett. **69**, 503 (1996).

[25] J. Elsner, R. Jones, M. I. Heggie, P. K. Sitch, M. Haugk, T. Frauenheim, S. Öberg, and P. R. Briddon, Phys. Rev. B **58**, 12571 (1998).

[26] C. Shi, P. M. Asbeck, and E. T. Yu, Appl. Phys. Lett. **74**, 573 (1999).

[27] For simplicity we have assumed line charge densities and the Read model for the calculation of the maximum phase shift.

[28] L. Houben, M. Luysberg, and T. Brammer, Phys. Rev. B **70**, 165313 (2004).

[29] J. Takeda, K. Takagi, T. Okabe, H. J. Ko, and T. Yao, Phys. Status Solidi C **1**, 678 (2004).